Astron. Astrophys. 334, 420–426 (1998)

ASTRONOMY AND ASTROPHYSICS

# Correlation properties of the diffuse light from COBE -*FIRAS* maps

**C. Burigana**[1] **and L. Popa**[1,2]

[1] Istituto TeSRE, Consiglio Nazionale delle Ricerche, Via Gobetti 101, I-40129 Bologna, Italy
[2] Institute of Space Sciences, R-76900 Bucharest-Magurele, Romania

Received 11 August 1997 / Accepted 2 March 1998

**Abstract.** We search for a cosmic component of the far-infrared and submillimetre background using the data from the COBE-*FIRAS* instrument. From the correlation properties of the diffuse light maps obtained after all the foregrounds and discrete source contributions have been removed, we claim that the *rms* brightness is given by $(\nu I_\nu)_{rms} \simeq 4 \times (\lambda/400\mu\mathrm{m})^{-3.1}\mathrm{nWm}^{-2}\mathrm{sr}^{-1}$ for $\lambda \geq 400\mu$m. At angular scales ranging from few degrees to few tens of degrees we find a steepening of the angular auto-correlation function with respect to the behaviour derived from galaxy surveys at smaller angular scales, becaming its spectral index $\gamma \approx 2$, in agreement with the indications inferred from galaxy catalogues at similar scales. In addition it is found that the genus distributions of the diffuse light maps are consistent with a random gaussian field with a coherence angle $\sim 5^\circ.9$, in agreement with COBE-*DMR*. These evidences support the extragalactic origin of the detected residual far-infrared background.

**Key words:** cosmic microwave background – large-scale-structure of Universe – diffuse radiation – infrared: galaxies

## 1. Introduction

The cosmic far-infrared and millimetre background (CFIR/mm) should contain cumulative information pertaining to pregalactic, protogalactic and galactic systems. Measuring this background can give important information about the evolution of the Universe between the redshift of the last scattering and today (see e.g. Treyer et al. 1993; Franceschini et al. 1994).

Numerous models have been developed to predict the properties of CFIR/mm (Bond et al. 1986; Cole et al. 1992; Franceschini et al. 1994). These properties depend mainly on the cosmological density parameter, the evolution function of the galaxies and their clustering pattern and the primordial power spectrum of the density field.

The main difficulties of a direct measurement of the CFIR/mm background arise mainly because of the foregrounds removal in a model dependent and controversial way and of the statistical bias given by the observational uncertainties of the far-infrared/mm data. The lack of the distinct spectral signature of CFIR/mm is due to the existence of different possible contributors to this background, to their evolution with the cosmic redshift, $z$, and to the importance of re-processing of the star light by dust in our galaxy and in different types of galaxies (Mazzei & De Zotti 1996).

The direct analysis of the COBE-*DIRBE* data gives limits on the cosmic infrared background from the darkest parts of the sky (Hauser et al. 1995) ranging from 15 to 104 $\mathrm{nWm}^{-2}sr^{-1}$ for J, K and L bands. New upper limits at the level of (10-15) $\mathrm{nWm}^{-2}\mathrm{sr}^{-1}$ have been announced by the *DIRBE* team (Kashlinsky et al. 1996).

Recently Puget et al. (1996) suggested the existence of a cosmic far-infrared background component in *FIRAS* data in the 400-800$\mu$m range, with a spectrum that indicates the possible presence of sources at high redshift. Also, an isotropic component with similar spectral shape was found in *FIRAS* data by Fixsen et al. (1996), at an intensity level in agreement within a factor of $\simeq 1.5$ with that claimed by Puget et al. (1996).

Upper limits of the dark sky surface intensity from COBE-*FIRAS* maps have been also recently announced by Shafer et al. (1997); they are obtained by a technique that analyses for spatially correlated errors in the *FIRAS* data.

For the purpose of this work we took the advantage of the continuous spectral coverage of COBE-*FIRAS* data that permits the foregrounds removal and in the same time the measurement of the angular correlation function of the diffuse light.

The method based on the correlation properties of the diffuse light was also successfully applied in V (Shectman 1974) and UV (Martin & Bowyer 1989) bands and by the *DIRBE* team (Kashlinsky et al. 1996,1997).

We choose the frequency range between 300 and 1500 GHz as best spectral window. Our choice is motivated by the frequency dependence of the *FIRAS* instrumental noise that becomes an important bias factor above 1500 GHz and because the ratio of CFIB/mm to foregrounds increases with wavelength (Franceschini et al. 1994).

We take the data from LLSS and RHSS *FIRAS* independent modes and construct (after the subtraction of all foregrounds) low-noise maps used to measure the surface intensity distribution and the power spectrum of the diffuse background light, which is found to be in agreement with the idea that it is produced by matter clustered like galaxies.

(Throughout this paper we express the frequency $\nu$ in GHz and the surface intensity $I_\nu$ in MJy/sr; the conversion in brightness units is $1\,\mathrm{nW\,m^{-2}sr^{-1}} = 0.3\,\nu\,\mathrm{cm^{-1}\,MJy\,sr^{-1}}$).

## 2. Theoretical preliminaries

The infrared background originates from a variety of sources. Just a small fraction is coming from distant faint galaxies and is expected to contain information on the details of their formation and evolution.

As the most of the cosmological models assume that the large-scale structure forms as a result of the gravitational evolution of the initial Gaussian fluctuations of the primordial density field, the spatial galaxy correlation function $\xi(r)$ or equivalently the power spectrum $P(k)$ define the statistical properties of the density field. They are related through:

$$\xi(r) = \frac{1}{2\pi^2}\int_0^\infty P(k) j_0(kr) k^2 dk\,,$$

where $j_n(x)$ is $n$-th order Bessel function.

The contribution from early type of galaxies to the infrared background is expected to exibit angular correlations that reflect their spatial correlations (Shectman 1974; Cole et al. 1992). The angular autocorrelation function of the extragalactic background is defined as :

$$C(\vartheta) = < \nu\delta I_\nu(x)\cdot\nu\delta I_\nu(x+\vartheta) >, \quad (1)$$

where $\delta I_\nu = I_\nu - < I_\nu >$ is the map of surface intensity fluctuations at the frequency $\nu$ produced by a population of emitters.

The autocorrelation function C($\vartheta$) is related with $\xi(r)$ via the Limber equation (Peebles 1980, Kashlinsky et al. 1996):

$$C(\vartheta) = \int_0^\infty A_\vartheta(z)\left(\frac{d\nu I_\nu}{dz}\right)^2 \Psi^2(z)(1+z)^2\sqrt{1+\Omega z}\,dz, \quad (2)$$

where it was assumed the small angle approximation ($\vartheta \ll 1$) and null cosmological constant $\Lambda$; $\Omega$ is the density in units of the critical density; $\Psi(z)$ is a function that accounts for the evolution of the clustering pattern and is defined to be unity at $z = 0$; $A_\vartheta(z)$ relates directly to $\xi(r)$ (Peacock 1991, Kashlinsky 1992, Kashlinsky et al. 1997) through:

$$A_\vartheta(z) = 2R_H^{-1}\int_0^\infty \xi\left(\sqrt{u^2 + \frac{x^2(z)\vartheta^2}{(1+z)^2}}\right) du, \quad (3)$$

where $x(z)$ is the comoving distance, $R_H = cH_0^{-1}$, $H_0$ being the Hubble constant, and $u = cdt/dz$.

After the convolution of Eq. (2) with the *FIRAS* beam that has FWHM $\tau = 7^\circ$, the autocorrelation function at zero-lag $C(0)$ can be written as (Kashlinsky et al. 1996):

$$C(0) = \int_0^\infty A_\tau(z)\left(\frac{d\nu I_\nu}{dz}\right)^2 \Psi^2(z)(1+z)^2\sqrt{1+\Omega z}dz, \quad (4)$$

where $A_\tau(z) = (1/(2\pi R_H))\int_0^\infty P_0(k) k\, W(kx(z)\tau/(1+z))\,dk$, $P_0(k)$ is the power spectrum of the galaxy clustering at the present epoch, and $W(x) = (3j_1(x)/x)^2$ define the window function of the beam.

Eq. (4) can be used to place an upper limit on the rms brightness of the diffuse light field (Kashlinsky 1992, Kashlinsky et al. 1996):

$$(\nu I_\nu)_{z,rms} \leq \sqrt{\frac{C(0)}{min(A_\tau(z))}}, \quad (5)$$

where $(\nu I_\nu)_{z,rms} = \int_0^\infty (d\nu I_\nu/dz)^2\Psi^2(z)(1+z)^2\sqrt{1+\Omega z}\,dz$. The small angle approximation, $\vartheta \ll 1$, is required to separate the angular dependence of the correlation function from the integral in Eq. (4). The numerical integration of Limber's equation shows that this factorization works quite well also to relatively higher separation angles ($\vartheta \sim 30^\circ$, Peebles 1980).

The analysis of the two-point correlation function obtained from APM galaxy catalogue (Maddox et al. 1990) shows at small angular scales a power law dependence of the correlation function, $C(\vartheta) \propto \vartheta^{-\gamma}$, with a spectral index $\gamma \simeq 0.7$. This implies for the underlying spatial correlation function $\xi(r)$ a power law behaviour $\xi(r) \propto r^{-1-\gamma}$ and a power spectrum $P(k) \propto k^{\gamma-2}$ (Kashlinsky 1992, Baugh & Efstathiou 1993).

The analysis of the APM data in different narrow magnitude ranges (Kashlinsky 1992) shows, in the assumption of the standard inflation model [$\Omega = 1$ and a primordial power spectrum of Harrison-Zel'dovich (HZ)], that the maximal wavenumber where the APM power spectrum can enter to the HZ regime is $k_0 \simeq 0.02h\mathrm{Mpc}^{-1}$ ($h = H_0/100\mathrm{Km/s/Mpc}$).

COBE-*FIRAS* beam sets scales corresponding to wavenumbers $k \lesssim 3\times10^{-3}h\mathrm{Mpc}^{-1}$. At these scales one can expect (Kashlinsky 1992) that the power spectrum of the extragalactic background is either close to the HZ regime, leading to a galaxy spatial correlation function close to $\xi(r) \propto r^{-4}$, either decreases with decreasing $k$ steeper than HZ power spectrum, or is a white noise power spectrum leading to $\xi(r) = 0$.

## 3. Data analysis

*FIRAS* is a four-port (two input, two output) Michelson Interferometer (COBE-*FIRAS* Explanatory Supplement 1995). A dichroic filter at each output port (arbitrarily named "Left" and "Right") splits the beam into "Low" (30-660) GHz and "High" (60-2880) GHz frequency bands producing spectra with a resolution of 4.2 GHz and 16.9 GHz respectively.

For the purpose of this work we took the data from LLSS and RHSS modes at low resolution. The data cover 95% of the sky with an angular resolution $FWHM = 7^\circ$.There are 6144 pixels with a pixel separation angle of about $2^\circ.6$.

Each pixel in the sky consists of a spectrum with 34 and 166 points for LLSS and RHSS modes respectively. All the spectra are complex with real and imaginary components stored separately. Typically observations are six months apart, but pixels near the ecliptic poles were observed more often. For pixels with multiple observations the spectra was averaged (weighted

by the number of interferograms IFGs) to produce an average spectrum per pixel.

The dispersion among the spectra for all pixels was averaged and the square root of the mean variance per IFG for the entire mission (referred as $C_{Vector}$ ) estimates the detector noise. $C_{Vector}$ has a frequency dependence, being an order of magnitude larger for RHSS than for LLSS. The weights used in the fitting procedures are obtained by considering the appropriate covariance matrix for high and low frequency channels (COBE-*FIRAS* Explanatory Supplement 1995; Shafer et al. 1997).

### *3.1. Foregrounds removal*

For each pixel in the maps we fit the spectra in the considered frequency range with different components assuming known spectral shapes.

1. A monopole spectrum modelled with a Planck function $B_\nu(T_0)$ at a temperature of $T_0 = 2.728$ ($\pm 0.009$K at the $1\sigma$ level, Mather et al. 1990, 1994, Fixsen et al. 1996).
2. A dipole spectrum fitted by the derivative of the Planck function with $T_d = 3.369$mK (Fixsen et al. 1996):
$$T_d \frac{\delta B_\nu}{\delta T} \times \cos(\Theta),$$
where $\Theta$ is the angle between the line of sight and the orientation of the cosmic dipole ($l = 264^\circ.16 \pm 0.15$ and $b = 48^\circ.26 \pm 0.15$). The variation of the $T_0$ values from pixel to pixel induces in the residual spectra an isotropic behaviour of the kind $\Delta T_0 \delta B_\nu(T_0)/\delta T$ for the frequencies $\nu \leq 350$ GHz (see also Shafer et al. 1997).
3. The contribution of the galactic dust described by using a spectral model with two modified blackbodies (for "cold" and "warm" galactic dust contributions) and a $\nu^2$ emissivity law:
$$\tau_{cold} \left(\frac{\nu}{\nu_0}\right)^2 B(\nu, T_{cold}) + \tau_{warm} \left(\frac{\nu}{\nu_0}\right)^2 B(\nu, T_{warm}), \quad (6)$$
where $\tau_{cold}$ and $\tau_{warm}$ are the optical depths and the characteristic frequency $\nu_0$ is 900 GHz (Reach et al. 1995). We found that this dust spectral model gives the best description of our data in terms of the $\chi^2$.
The spectral lines were fitted and removed using the appropriate data files containing the spectral intensities and line shapes.
4. The contribution of the Zodiacal light present at high frequencies was modelled for each *FIRAS* pixel by taking the $25\mu$m *DIRBE* latitude profile scaled by $0.167(\nu/100\mu\mathrm{m})^{-3}$ (Reach et al. 1995; Puget et al. 1996).

The residual spectra obtained for each pixel are characterized by a number of bright discrete sources that must be eliminated. We use for this purpose the wavelets filtering of the spectra. The wavelet transform is a linear operation that generates a data structure which contains scales of various lengths, the wavelet base functions being quite localised in space. The wavelet coefficients define a transformation matrix that is used in a pyramidal algorithm acting like quadrature mirror filter pair (Press et al. 1992). The residual spectra from each pixel, for the considered frequency window, was wavelet transformed and than reconstructed after the frequency channels with the brightness above same clipping threshold have been blanked together with the frequency adjacent channels. The same cut was applied to all the four neighbour pixels. The clipping threshold is defined like a factor relative to the standard deviations and is the same for the pixels in the same map. We tested different clipping thresholds of 2, 3, 3.5, 4 and 4.6. The threshold values of 2.5 for LLSS and 4.6 for RHSS maps were retained as satisfying the following requirements:
- the distribution of the residual intensities, after the mean has been subtracted, approaches a gaussian distribution;
- the rms surface intensity value at each frequency is above the corresponding *FIRAS* instrumental noise, $\sigma_{noise}$, defined by $\sigma_{noise} = C_{Vector}/\sqrt{N}$, where N is the total number of interferograms.

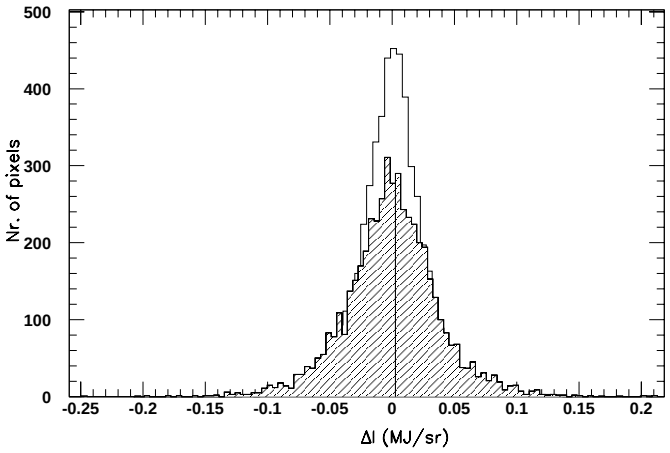


**Fig. 1.** The histograms of the residual surface intensity with the mean subtracted for LLSS (filled) and RHSS maps

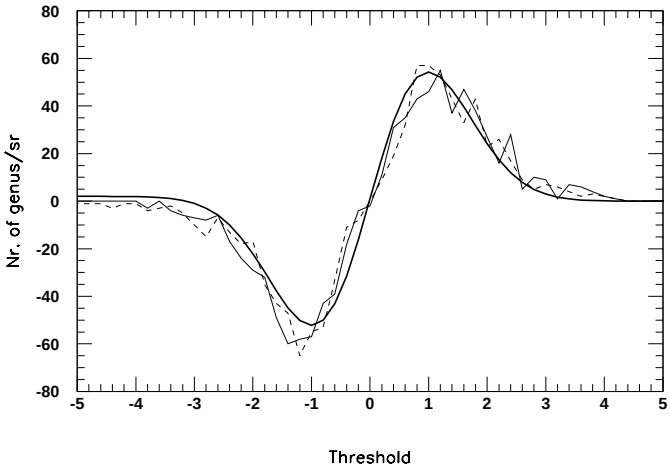


**Fig. 2.** The genus distribution for LLSS (solid thin line) and RHSS (dashed line); our best fit (solid thick line)

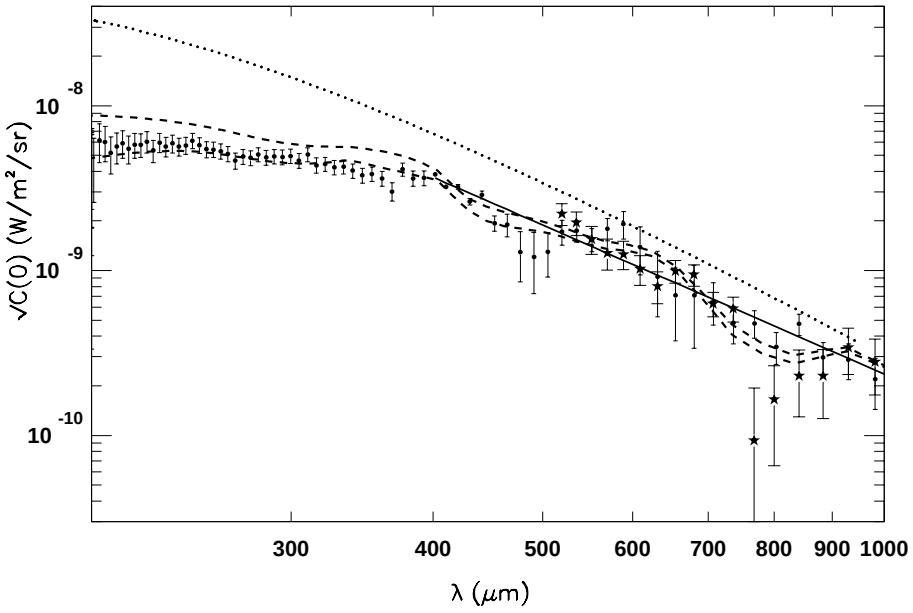


**Fig. 3.** $\sqrt{C(0)}$ as a function of wavelength for LLSS (stars) and RHSS (filled points) and our corresponding power law best fit for $\lambda \geq 400\mu$m (solid line); upper limit from Shafer et al. (1997) (dotted line); the residual brightness found by Puget et al. (1996) (dashed lines) without (upper curve) and with (lower curve) subtraction for ionized gas.

### *3.2. Properties of the residual component*

The histograms of the residuals obtained after the averages removal, for both high and low frequency maps, are presented in Fig. 1.

The residuals obtained in this way were used to construct weighted averaged maps over the frequency window considered for both LLSS and RHSS. In this way the correlations existing between adjacent frequency channels are reduced.

If the diffuse light retained in the averaged maps has a cosmological origin, its fluctuations have to reflect Gaussian density perturbations with random phases. To test this hypothesis we analysed the topological structure of the maps. We examined the distribution of spots with the intensity above same threshold (expressed in units of standard deviation) and found that the histograms are skew, with a clear gaussian shape.

We have used another useful topological discriminator, the number of genus defined as the excursion regions enclosed by isobrightness contours (Gott et al. 1990). The genus per unit solid angle is a locally invariant quantity. For a random Gaussian field with the rms brightness fluctuation $\sigma$ the expectation value of the total genus is: $G_S = 4\pi g + erfc(\nu/\sqrt{2})$ where $erfc$ is the complementary error function, $\nu$ is the threshold expressed in number of $\sigma$ and $g$ is the mean genus per unit area, $g = (2\pi)^{-3}(\nu/\vartheta_c^2)e^{-\nu^2/2}$, and $\vartheta_c$ is the coherence angle of the field.

Fig. 2 presents the genus distribution obtained for the high and low frequency maps averaged in 400-600 GHz and 400-1500 GHz bands respectively.

The shapes of the genus distributions are typical for a random Gaussian field with a coherence angle $\vartheta_c = 5^\circ.9$, in good agreement with the results obtained from the *DMR* data based on the analysis of temperature correlation function.

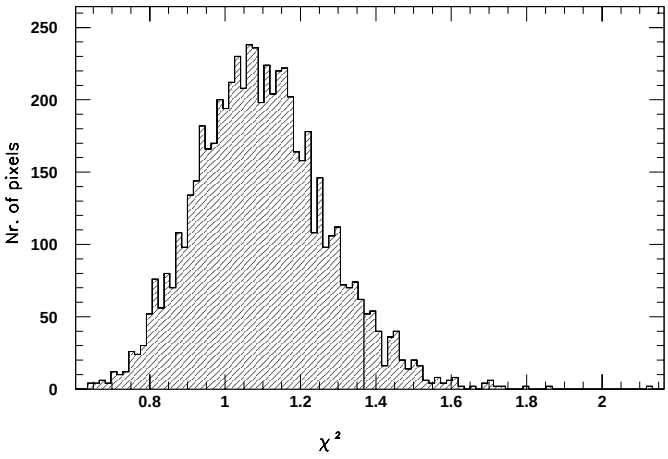


**Fig. 4.** The $\chi^2$ distribution

## 4. Results

### *4.1. Correlation properties of the diffuse light*

The upper limits on the fluctuations of CFIB/mm offer a powerful test of any model of its sources.

These upper limits were calculated as the rms surface intensity (with the mean subtracted) at each frequency by selecting those pixels that satisfied the conditions already mentioned.

We analyzed the frequency dependence of $\sqrt{C(0)}$ for different fields: two $20^\circ \times 20^\circ$ regions centred on the ecliptic poles, a $10^\circ \times 10^\circ$ field around the Lockman region (l,b)=$(148^\circ, 53^\circ)$ (for these fields the statistical error is smaller), two fields with $b > 60^\circ$ and $b < -60^\circ$ respectively, and the entire maps LLSS and RHSS excluding the pixels within $|b| \leq 10^\circ$.

For all the investigated fields we found a high isotropy of the $\sqrt{C(0)}$.

Fig. 3 presents the $\sqrt{C(0)}$ as a function of the frequency for high and low frequency maps. The plotted error bars are the

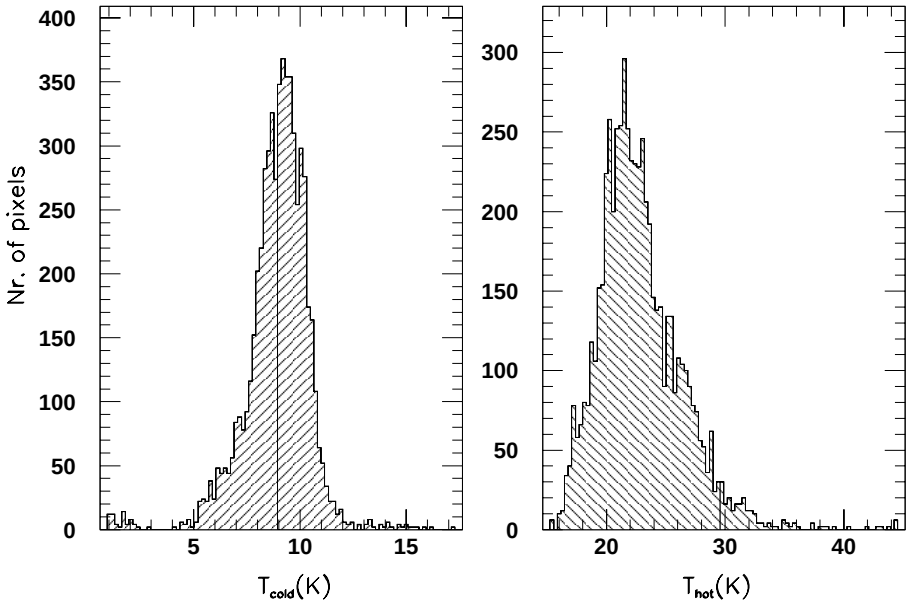


**Fig. 5.** Temperature distributions for the "cold" and "warm" dust components

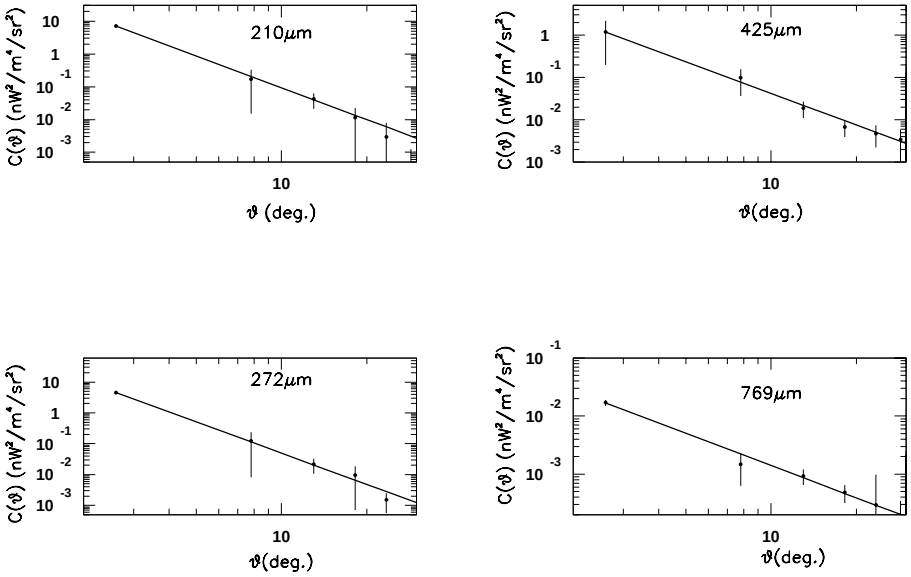


**Fig. 6.** Angular autocorrelation functions of submillimetre diffuse light (error bars at $1\sigma$ level) at $2.6^\circ < \vartheta \lesssim 30^\circ$ for several frequency bands, reported in each panel, together with the power laws that fit the corresponding data sets (solid line).

$1\sigma$ statistical errors. For an easy comparison with the previous results (Puget et al. 1996; Shafer et al. 1997) we present our results in terms of $\nu I_\nu$ versus $\lambda$.

Translated in upper limits for $(\nu I_\nu)_{rms}$ the frequency dependence of $\sqrt{C(0)}$ implies:

$$\sqrt{minA_\tau(z)} \times (\nu I_\nu)_{rms} \leq (3.64 \pm 0.02)$$

$$\times \left(\frac{\lambda}{400\mu\mathrm{m}}\right)^{-3.1\pm0.01} \mathrm{nWm}^{-2}\mathrm{sr}^{-1} \quad (7)$$

for $\lambda \geq 400\mu$m.

Although our approach is in principle devoted to find upper limits for $(\nu I_\nu)_{\rm rms}$, we refitted the experimental spectra by adding a new component with the same frequency dependence as $\sqrt{C(0)}$ obtained in this way, in order to give an estimate of the residual brigthness. From the entire maps ($|b| \geq 10^\circ$) we have found that:

$$(\nu I_\nu)_{rms} = (1.18 \pm 0.01)\sqrt{C(0)},$$

in good agreement with the results of Puget et al. (1996).
We present in Fig. 4 the $\chi^2$ distribution and in Fig. 5 the temperature histograms for the infered "cold" and "warm" dust components of the RHSS map. Introducing the CFIR/mm spectrum in our fit the dust components became well separated and the $\chi^2$ distribution fainter.

### *4.2. On the angular autocorrelation function*

We have derived the angular autocorrelations function $C(\vartheta)$ of submillimetre diffuse light in ten frequency windows of 100 GHz width by averaging over the frequency the LLSS and RHSS maps.

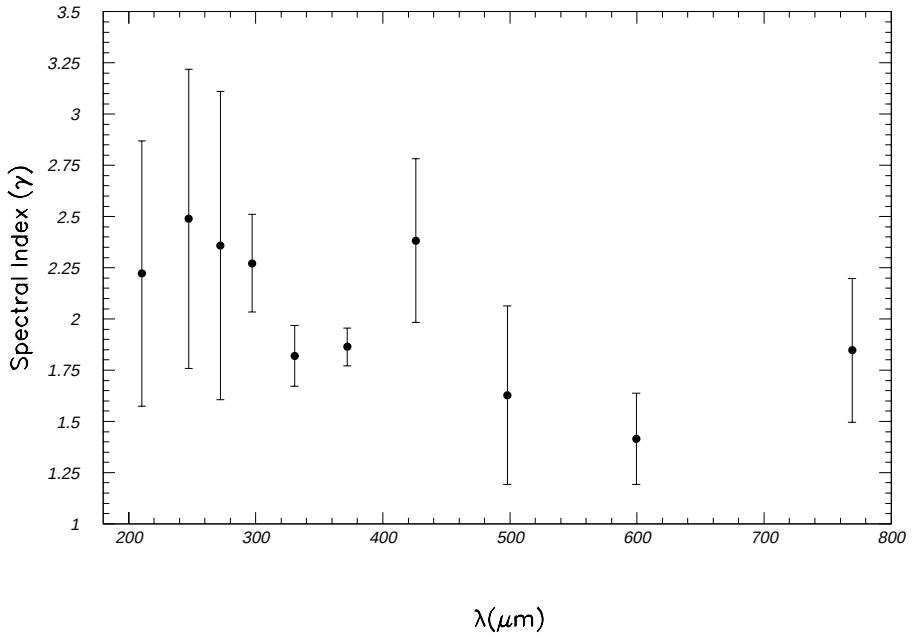


**Fig. 7.** Spectral indeces of angular autocorrelation function of submillimetre diffuse light at the ten considered frequency bands (error bars at $1\sigma$ level).

Fig. 6 shows our results for four typical channels in the angular range $2.6^\circ < \vartheta \lesssim 30^\circ$ when power law approximations [$C(\vartheta) \propto \vartheta^{-\gamma}$, solid lines] fit quite well the data.

Our uncertainty in the determination of the spectral index $\gamma$ at each band (see Fig. 7) is relatively large and we find a spreading of its value with the wavelength, ranging $\gamma$ from 1.2 to 3.2 (including $1\sigma$ error), with a possible steepening of the angular autocorrelation function with the frequency.

In spite of these uncertainties, our result is substantially in agreement with the evidence of a steepening of the galaxy angular autocorrelation function at scales larger than few degrees, found from the Lick survey and from the APM catalogue (Maddox et al. 1990, Baugh & Efstathiou 1993, Maddox et al. 1996). This evidence further supports the extragalactic origin of the detected diffuse light.

## 5. Conclusions

We have analyzed COBE/*FIRAS* maps searching for an isotropic foreground at submillimetre wavelengths. Our method is complementary to that followed by Puget et al. (1996), being based on the correlation properties of *FIRAS* maps and not requiring additional data sets to subtract the contribution of the Galaxy. By exploring different sky regions we have obtained residual components that are always in agreement one with each other; this fact, together with the good isotropy of the $\sqrt{C(0)}$, further supports the argument that the foregrounds are accurately subtracted. In addition, the residual maps so obtained are above the instrumental noises at each frequency with fluctuations consistent with random gaussian field: their genus distributions are in agreement with a random gaussian field with a coherence angle of $\sim 5.^\circ 9$ like that of the *DMR* maps. The high isotropy of this component can be interpreted as an effect of emission by a galactic halo at high distance from the galactic centre (Fixsen et al. 1996) or as an extragalactic integrated emission from distant galaxies (Puget et al. 1996, Franceschini et al. 1994) with a bulk of star formation rate at relevant redshift. The angular dependence of the autocorrelation function at scales ranging from few degrees to few tens of degrees presents a steepening (characterized by a spectral index $\gamma \approx 2$) with respect to the behaviour at smaller angular scales, in agreement with the indications derived from galaxy surveys at similar scales. This argument supports the idea of an extragalactic origin of this background, like that predicted by the model of Franceschini et al. (1994) which takes into account the galaxies luminosity evolution. The level and the power law dependence of this extragalactic component constrain the redshift (2.1–3.8) and the metallicity production rate of this active phase of star formation rate and dust reprocessing (Burigana et al. 1997) with implications for the level of discrete source fluctuations at millimetre and sub-millimetre frequencies (Toffolatti et al. 1998). These results can be used to constrain the galaxies evolution.

*Acknowledgements.* It is a pleasure to thank L. Toffolatti for useful discussions. We wish to acknowledge an anonymous referee for constructive comments and for the careful reading of the original text. LP wishes to thank to the Istituto TeSRE/CNR for the warm hospitality during her stay in Bologna. Part of this work was supported by the Human Capital and Mobility programme of the European Union, under Contract ERBCIPDCT 940019. The COBE data sets were developed by the NASA Goddard Space Center under the guidance of the COBE Science Working Group and were provided by the NSSDC.

## References

Baugh, C.M. & Efstathiou, G., 1993, MNRAS 265, 145
Bond, J.R. et al., 1986, ApJ 306, 428
Burigana, C. et al., 1997, MNRAS 287, L17
COBE-*FIRAS* Explanatory Supplement, ed. Mather, J.C. et al., (1995), COBE Ref. Pub. No.95-C

Cole, S. et al., 1992, ApJ 385, 9
Fixsen, D.J. et al., 1996, ApJ 473, 576
Franceschini, A. et al., 1994, ApJ 427, 140
Gott, J.R. et al., 1990, ApJ 352, 1
Hauser, M.G. et al. 1995,"Unveiling the Cosmic Infrared Background" ed. E.Dwek (in AIP Proc.)
Kashlinsky, A. 1992, ApJ 399, L1
Kashlinsky, A. et al., 1996, ApJ 470, 681
Kashlinsky, A. et al., 1997, "Diffuse Infrared Radiation and the IRTS" Conference, Kanagawa, Japan, November 1996 (preprint astro-ph/9701216)
Maddox, S. et al. 1990, MNRAS 242, 43
Maddox, S. et al., 1996, MNRAS 283, 1227
Martin, C. & Bowyer, S., 1989, ApJ 338, 677
Mather, J. et al., 1990, ApJ 354, L37
Mather, J. et al., 1994, ApJ 420, 439
Mazzei, P. & De Zotti, G., 1996, MNRAS 279, 535
Peacock, J.A., 1991, MNRAS 253, 1
Peebles, P.J.E. 1980, "Large Scale Structure of the Universs", Princeton Univ. Press.
Press, W. et al., 1992, "Numerical Recipes in Fortran", Cambridge Univ. Press
Puget, J. L. et al., 1996, A&A 308, 5
Reach, W.T. et al., 1995, ApJ 451, 188
Shafer, R. A. et al., 1997, preprint, submitted to ApJ.
Shectman, S. 1974, ApJ 188, 233
Toffolatti, L. et al., 1998, MNRAS, in press (preprint astro-ph/9711085)
Treyer, M. et al., 1993, ApJL 408, L1